Statistical Analysis of the Uncertainties in Cloud Optical Depth Retrievals Caused by Three-Dimensional Radiative Effects

Tamás Várnai and Alexander Marshak
Joint Center for Earth Systems Technology of
NASA Goddard Space Flight Center and
University of Maryland, Baltimore County

Prepared for the Journalof the Atmospheric Sciences
May 10, 2000

Corresponding author address: Tamás Várnai, Code 913, NASA GSFC, Greenbelt, MD 20771, USA. E-mail: varnai@climate.gsfc.nasa.gov

Abstract

This paper presents a simple approach to estimate the uncertainties that arise in satellite retrievals of cloud optical depth when the retrievals use one-dimensional radiative transfer theory for heterogeneous clouds that have variations in all three dimensions. For the first time, preliminary error bounds are set to estimate the uncertainty of cloud optical depth retrievals. These estimates can help us better understand the nature of uncertainties that three-dimensional effects can introduce into retrievals of this important product of the MODIS instrument. The probability distribution of resulting retrieval errors is examined through theoretical simulations of shortwave cloud reflection for a wide variety of cloud fields. The results are used to illustrate how retrieval uncertainties change with observable and known parameters, such as solar elevation or cloud brightness. Furthermore, the results indicate that a tendency observed in an earlier study—clouds appearing thicker for oblique sun—is indeed caused by three-dimensional radiative effects.

1. Introduction

Satellite measurements of the solar radiation reflected by clouds are often used to retrieve cloud properties such as the amount of liquid water in the clouds and the size of cloud droplets. Current retrieval algorithms are based on one-dimensional (*1D*) radiative transfer theory, which assumes that there is a one-to-one relationship between cloud reflective and physical properties. Common everyday experience, however, tells us that clouds often feature fully three-dimensional (*3D*) structures with strong variabilities in both horizontal and vertical directions. Radiative interactions among nearby elements of heterogeneous clouds can upset the one-to-one relationships between cloud reflection and physical properties, so any measured brightness can be associated with a variety of cloud properties. Current retrievals avoid potential ambiguities by ignoring 3D effects and using the clear relationships of 1D radiative transfer instead—but as numerous theoretical studies (e.g., Davies 1984, Kobayashi 1993, Barker and Liu 1995) and several observational results (e.g., Loeb and Davies 1996, Loeb and Coakley 1998) indicate, this can introduce significant errors into the retrievals. A different approach to resolving retrieval ambiguities is to determine not a single best-guess value, but rather, the statistical parameters of the distribution of possible values. This approach has been used recently to estimate leaf area index and the photosynthetically active radiation from space

(Knyazikhin et al. 1998a, Diner et al. 1999). The current paper examines this statistical approach for cloud optical thickness retrievals, focusing on the uncertainties that horizontal cloud variability introduces into retrievals based on 1D theory. This study thereby complements earlier studies that examined the influence of vertical cloud heterogeneities (e.g., Li et al. 1994, Platnick 1997).

Understanding the effects of using 1D radiative transfer theory is especially important, because recent improvements in measurement accuracy can lead to comparable improvements in retrieval accuracy only if the retrievals account for all relevant physical processes (Figure 1). However, while the possibility that 3D effects can cause significant retrieval errors is widely accepted, the magnitude of these errors in various situations is yet to be determined. This paper presents a first attempt toward this goal: It describes a simple approach to assessing the influence of horizontal cloud variability on the operational processing (Nakajima and King 1990, King et al. 1997) of measurements by the Moderate Resolution Imaging Spectroradiometer (MODIS) instrument on board the TERRA satellite. In particular, the study examines the probability distribution of retrieval errors for stratocumulus cloud optical depth and describes a simple technique to set error bounds for the MODIS retrievals. Figure 2 illustrates these error bounds and shows that while such error bounds cannot determine the retrieval errors for individual pixels (for example, they do not show that the optical

thickness is often overestimated on the sunlit slopes on the left side of cloud bumps and underestimated on the shadowy slopes on the right side), they can give statistically representative estimates on the magnitude of the errors.

The outline of this paper is as follows: First, Section 2 describes the test dataset used in the proposed assessment algorithm. Then, Section 3 outlines the algorithm's basic approach and also uses radiative transfer simulation results to highlight various features of the retrieval errors. Finally, Section 4 summarizes the paper's main conclusions and outlines some possible directions for future work.

2. Test dataset

Since the proposed technique is based on a climatology of 3D effects that are obtained through radiative transfer simulations, it is very important to ensure that the simulations be representative of the processes that occur in the real atmosphere. The key issue is not whether 3D radiative processes can be calculated accurately—results from the I3RC project (Cahalan et al. 1999) strongly suggest that the Monte Carlo radiative transfer code used in this study is highly accurate—but whether the set of examined clouds is truly representative of the real clouds observed by satellites.

The biggest challenge in building a climatologically representative set of 3D cloud fields is that there are no suitable measurements of full 3D cloud structures. In-situ aircraft measurements give only 1D transects, and passive measurements of the radiation leaving a cloud field cannot give detailed information on internal cloud structure. In addition, these passive measurements can be affected by the very same 3D effects we are trying to understand. Although in principle, active sensors (i.e., lidars and cloud radars) could determine 3D cloud structures, current systems give information only in the vertical and one horizontal direction, leaving cloud variability in the other horizontal direction unknown. Evans et al. (2000) presented a first attempt to overcome this limitation by developing a stochastic cloud model to extend the measured cloud fields to the unknown horizontal dimension. The present study examines the radiative properties of 3D cloud fields that were generated by a variety of stochastic cloud models: the bounded cascade model (Cahalan et al. 1994, Marshak et al. 1994), the fractional integration model (Schertzer and Lovejoy 1987), and a slightly modified version of the fractional Brownian motion model as in Barker and Davies (1992).

Although the examined stratus/stratocumulus cloud fields were generated artificially, they incorporate knowledge obtained by observations in two ways. First, the models were created so that they reproduce systematic features observed in real clouds, most notably their power-law scaling (e.g., Cahalan and Snider 1989, Davis et al. 1994).

The simple scaling (also called self-affinity) means that the average change in cloud properties (e.g., optical depth) over distances Δx and $\lambda\Delta x$ (with $\lambda > 0$) can be related through (e.g., Vicsek, 1989, p. 33)

$$\left\langle \left| \tau(x) - \tau(x + \lambda\Delta x) \right| \right\rangle \sim \lambda^H \left\langle \left| \tau(x) - \tau(x + \Delta x) \right| \right\rangle \qquad (1)$$

where the ~ sign means statistical equality and < > indicates ensemble averaging over many realizations. The scaling parameter $H \in [0,1]$ characterizes spatial correlations in cloud properties. ($H = 0$ corresponds to jumpy, discontinuous statistical processes, while $H = 1$ indicates an almost everywhere differential process.) Typical H values for stratocumulus clouds are between 0.25 and 0.4, usually close to 1/3 (Marshak et al. 1997).

Secondly, real observations were also used in stochastic cloud modeling by choosing the models' input parameters such that they represent the observed average characteristics and variability of cloud properties. Because the main goal for this study was to generate a set of scenes that seeks to cover the natural variability of stratocumulus cloud properties, the clouds range from thin to thick, from almost homogeneous to very heterogeneous, from overcast to partially cloudy, and from flat to bumpy. Thus, all results presented in this paper are based on simulations for at least 300 scenes that each cover $(51.2 \text{ km})^2$ areas at 50 m resolution. Each scene was generated using a different random number sequence and a different set of cloud variability parameters. The

variability parameters were chosen for each scene according to a random uniform distribution that is based on the range of variability reported in Barker et al. (1996) (see Table 1). Backward Monte Carlo simulations then calculated the reflection of 10 randomly chosen pixels in each scene—and so the presented results are all based on simulations for at least 3,000 pixels.

Once a comprehensive dataset of such scenes is put together, realistic statistics of 3D radiative effects can be calculated by weighting data points from each scene according to how often the scene's parameters can be observed in real clouds. (As a result, data from scenes resembling typical clouds will receive large weights, whereas data from scenes similar to rare clouds will carry much less weight in the statistical calculations.) For an easier illustration of the proposed technique, all data points in this paper are displayed with an equal weight and are accordingly given equal weight in the statistical calculations. Sensitivity studies (not shown) indicated that while applying realistic weighting schemes (e.g., assigning less weight to increasingly heterogeneous scenes) can change the mean and standard deviation of retrieval errors, it does not modify the qualitative features discussed in this paper. In the future, we plan to calculate climatologically representative statistics on retrieval errors for several specific locations (such as the Atmospheric Radiation Measurement (ARM) program site in central

Oklahoma and in the Western Pacific) by comparing the variability of simulated scenes to variabilities observed in cloud radar measurements.

The presented simulations assume nonabsorbing cloud droplets with a C.1 phase function and do not consider the effects of cloud-free air and the underlying surface. The cloud fields are specified at a 50 m resolution, below which scale the fields are assumed to be homogeneous. The results of Marshak et al. (1998) show that using this assumption does not significantly change the calculated cloud radiative properties. Most simulations presented in this paper, however, obtained cloud reflection for $(250\ m)^2$ pixels, thereby matching the resolution of the MODIS instrument. Except when noted otherwise, all presented results are for 60° solar zenith angle.

3. Estimation of retrieval uncertainties

3.1 Magnitude of retrieval errors

As mentioned in the introduction, the main goal of the presented technique is to estimate the influence of 3D radiative effects on MODIS optical depth retrievals and to set error bounds on the retrieval results accordingly. The algorithm proposed to set the error bounds is illustrated in Figure 3, which displays simulation results for a wide range

of clouds. The operational MODIS algorithm works by determining which cloud optical thickness can yield the measured reflectivity value according to 1D radiative transfer theory, i.e., according to the solid line in Figure 3. The proposed assessment technique then estimates the retrieval uncertainty by considering a narrow brightness interval around the observed radiance (which represents the measurement accuracy and is indicated by horizontal dashed lines in the figure) and calculating how spread out the true optical thickness values yielding brightnesses inside the narrow interval are in the 3D simulations.

Figure 4 shows that generally, the standard deviation (σ) of the τ-retrieval errors (ε)—defined as

$$\sigma = \frac{1}{N-1}\sqrt{\sum_{i=1}^{N}\left(\varepsilon_i - \langle\varepsilon\rangle\right)^2}, \tag{2}$$

with N being the number of pixels—increases with cloud reflectivity. This tendency is consistent with the findings of Pincus et al. (1995), who showed that retrieval errors caused by factors other than 3D effects increase with cloud brightness as well. The initial increase seems fairly intuitive, because the influence of 3D effects (which push the individual points away from the 1D curve) increases with the original 1D brightness it modifies. At larger brightnesses the increase accelerates because of the flattening of the 1D curve in Figure 3: Since the brightness hardly changes with τ for thick areas, a given

large brightness can occur for a wide range of τ values. This can be interpreted as a sign that at bright (that is, thick) regions, the optical thickness and reflectivity (I) become decoupled from each other, and the brightness is determined not as much by τ, as by the local geometry that creates 3D effects (e.g., whether the examined slope tilts toward or away from the sun). Finally, the spread of retrieval errors remains fairly constant at the brightest regions, because the 1D optical thickness retrievals are constrained by the arbitrary limit of not retrieving optical thicknesses greater than 100. Thus, further increases in cloud brightness do not lead to larger retrieval errors.

3.2 Magnitude and sign of retrieval errors

In addition to cloud brightness, retrieval uncertainties also depend on other factors, such as the sun-view geometry and the spatial resolution of reflectivity measurements. For example, Figure 5 shows that, in agreement with the findings of earlier studies (e.g., Chambers et al. 1997, Davis et al. 1997, Zuidema and Evans 1998), the influence of 3D effects decreases with coarsening resolution, and at really coarse resolutions a 1D heterogeneity effect called the plane-parallel bias (Cahalan et al. 1994) becomes dominant. As a result, retrievals can be expected to be most accurate at intermediate resolutions in the order of a few hundred meters to a few kilometers (Davis

et al. 1997). However, as Figure 6 shows, retrieval errors due to 3D effects increase sharply for more oblique illuminations. This tendency causes the overestimations that are due to 3D effects to dominate over the underestimations that are due to the plane-parallel bias, even at resolutions as coarse as 30 km (Loeb and Davies 1996).

Examination of the cumulative histogram of retrieval errors,

$$F(\Delta\tau) = Prob(Error < \Delta\tau), \tag{3}$$

can offer additional insights into the influence of 3D effects. Figure 7 shows that the cumulative histogram value of 0.5 occurs for retrieval errors close to 0, which means that underestimations and overestimations occur about equally often. This is especially informative for oblique sun, because it indicates that the 3D effects are caused primarily by short-range interactions among nearby cloud elements. (If large scale interactions had dominated, thick areas would have cast long shadows, causing underestimations for large areas behind them and thus making underestimations more frequent than overestimations.) The figure also shows that when only large retrieval errors are considered, underestimations are more frequent for high sun and overestimations prevail for oblique sun. This is consistent with the sign of overall biases that are apparent in Figure 6.

On the topic of systematic retrieval biases, Figure 8 shows the relationship between the mean optical thickness of all pixels that have a certain nadir reflectivity in 3D simulations

$$\bar{\tau}_{3D}(I) = E(\tau \mid \text{reflectivity} = I), \tag{4}$$

where E is the mathematical expectation and the optical thickness retrieved using 1D theory ($\tau_{1D}(I)$). The figure suggests that 1D retrievals give unbiased results for pixels that are not too bright. For brighter areas, however, using 1D theory results in an overestimation of the true mean optical thickness: When 3D effects enhance the brightness of thick slopes tilted towards the sun, 1D retrievals do not know about the tilting and must therefore assume very large optical thicknesses to account for the large brightness values. The fact that overestimations increase with cloud brightness is consistent with the observations of Loeb and Davies (1996) further supports their assertion that the biases they observed are indeed caused by 3D radiative effects.

The fact that τ retrievals based on single reflectivity values cannot yield accurate results for thick or bright areas is also illustrated in Figure 9. The figure shows that the

$$I_{mean}(\tau) = E(I_{3D} \mid \text{optical depth} = \tau) \tag{5}$$

and the $\tau_{mean}(I)$ curves diverge for $\tau > 25$ (i.e., $I > 0.65$), indicating that the mean τ-I relationship becomes nonreversible (Knyazikhin et al. 1998b).

In addition to considering the basic statistics of the true τ distribution as a function of cloud brightness, one can also examine the full τ histograms for fixed I values (Figure 10). (Similar histograms of leaf area index values can be found in Knyazikhin et al. (1998a).) The histograms clearly illustrate the tendency shown in Figure 4: that the brighter a pixel is, the wider the histogram of possible τ_{true} values is, and so the harder it is to estimate the pixel's true optical depth. Figure 10 also shows that the histograms can be quite asymmetric, i.e., underestimations and overestimations follow different probability distributions. This asymmetry is especially noticeable for dark pixels (I = 0.3), where the histogram's tail on the left side is almost completely missing. (This tail contains pixels that are extra bright because they are on a sunlit slope.) Naturally, any tail on the left is limited by the fact that τ cannot go below zero. However, Figure 10 shows that the histogram does not reach this limit, which means that another factor must restrict the tail on the left side well above the zero value. The fact that the tail on the left is smaller for less bright pixels can be explained as follows: While a pixel in bright (and generally, thick) areas can gain significant extra illumination if the pixel in front is thinner, a pixel in a darker (and generally thinner) area is not affected much by having a thinner pixel in front, because even if the neighbor in front were not thinner, it would still be fairly thin (like our pixel) and would allow plenty sunlight to reach the side of our pixel.

The main practical implication of the resulting skewness is that since the distribution of retrieval errors is asymmetric, optimal error bounds should be set differently for underestimations and overestimations. This implication is illustrated in Figure 11, which shows the histograms of the differences (τ_{true} - $\tau_{retrieved}$). τ_{true} can be considered a random variable corresponding to random pixels with brightesses in a narrow interval around the I = 0.6 value, and $\tau_{retrieved}$ can be considered a deterministic number retrieved from I = 0.6 using 1D radiative transfer. The figure shows that the standard deviation is strongly influenced by the few pixels with large difference values, and as a result, when the actual difference distribution is approximated by a Gaussian curve, this curve will be too wide. Consequently, while the [-σ,σ] interval between the dotted lines would contain 68% of the data according to the Gaussian curve, the interval contains a much higher percentage of points in the actual distribution.

The correct error bounds were calculated following standard statistical techniques (e.g., Cowan 1998, p. 119). These empirical error bounds were set to ensure that the error for a randomly selected pixel lies inside the bounds with a 95% or 68% probability (which we denote by α), and lies outside the bounds on either side with a probability of (1-α)/2 (= 0.025 and 0.16 for α = 0.95 and 0.68, respectively). In practice, the bounds for underestimation (B_u) and overestimations (B_o) were determined empirically from the equations

$$\int_{-\infty}^{B_u} P(\Delta\tau)\, d(\Delta\tau) = \frac{1-\alpha}{2} \tag{6}$$

and

$$\int_{B_u}^{\infty} P(\Delta\tau)\, d(\Delta\tau) = \frac{1-\alpha}{2}. \tag{7}$$

where P is the probability density function.

Figure 12 shows the error bounds calculated empirically for underestimations and overestimations, as well as the bounds estimate using the Gaussian assumption. The figure indicates that often there are significant differences between the three error bounds. (The saturation of overestimation error bounds can be attributed to the fact that retrievals are limited optical thicknesses smaller than 100.) The figure also shows that the underestimation error bounds drop to zero at bright areas, which indicates that underestimations become very rare in these areas and occur for a smaller percentage of pixels than the percentage that one would expect to be excluded by the 95% and 68% level error bounds on each side of the error histogram (2.5% and 16%, respectively).

4. Conclusions

This paper presented results from a study that seeks to estimate the uncertainties that arise in satellite retrievals of cloud optical depth because retrievals are based on 1D

radiative transfer theory and thus do not consider the effects of horizontal cloud variability. As a first step toward this goal, the paper examined the probability distribution of retrieval errors due to heterogeneity effects, as obtained from radiative transfer simulations over a wide variety of heterogeneous scenes. Based on the simulated scenes, the RMS error of optical thickness retrievals for (1 km)^2 pixels were estimated to be in the range of 3 to 5 for a solar zenith angle of 60°. The estimated error distributions were used to develop a simple technique that can set error bounds for operational cloud property retrievals. Figure 13 illustrates an example of error bounds estimated by applying the technique to MODIS Airborne Simulator measurements.

The simulation results indicated that the retrieval uncertainties due to 3D radiative effects tend to increase with cloud brightness and solar zenith angle. For example, retrievals for 60° solar zenith angle gave unbiased overall averages for areas with nadir reflectivities less than 0.6, but the average optical thickness was increasingly overestimated for brighter regions. This behavior is consistent with the observations of Loeb and Davies (1996) and provides a further indication that the biases they observed were indeed caused by 3D radiative effects.

Although the results showed that retrievals over relatively dark areas can be expected to be free of overall biases, the results also indicated that these areas can still be affected by another complication: that retrieval errors have skewed probability

distributions. This finding is important when the uncertainty is characterized by error bounds for specific confidence levels, since it shows that optimal error-bounds should be set separately for underestimations and overestimations.

While the scenes used in the calculations cover a wide range of observed cloud field properties, they cannot be considered climatologically representative, since it is not known which scenes are important because they resemble real clouds that occur frequently and which scenes are less important because they resemble very rare clouds. Thus, the next step in quantitatively estimating the uncertainties of satellite retrievals will be for us to assign weights to the simulated scenes by comparing their structure to radar measurements over the ARM site in central Oklahoma and in the Western Pacific.

Finally, we plan to extend the presented approach so that it estimates retrieval uncertainties by considering not only the brightness of each pixel, but also the spatial, angular, and spectral variability of cloud reflection. Our current efforts seek to determine whether the influence of 3D effects can be estimated using the phenomenon that 3D effects enhance local brightness variability more strongly at absorbing than at non-absorbing wavelengths (Oreopoulos et al. 2000). Promising preliminary results suggest that the reliability of estimated error bounds can be greatly improved by comparing the local variabilities measured at 0.6 μm and at the new MODIS wavelength at 1.6 μm.

Acknowledgments

We appreciate funding for this research from the NASA EOS Project Science Office at the Goddard Space Flight Center (under grant NAG5-6675) and support from project scientist David O'C. Starr. We are also grateful to Yuri Knyazikhin, Anthony Davis, Steve Platnick, and Robert Pincus

for many fruitful discussions and to Laura Atwood for proofreading the manuscript and providing helpful suggestions.

References

Barker, H. W., and J. A. Davies, 1992: Solar radiative fluxes for stochastic, scale-invariant broken cloud fields. *J. Atmos. Sci.*, **49**, 750–761.

Barker, H. W., and D. Liu, 1995: Inferring optical depth of broken clouds from Landsat data. *J. Climate*, **8**, 2620–2630.

Barker, H. W., B. A. Wielicki, and L. Parker, 1996: A parameterization for computing grid-averaged solar fluxes for inhomogeneous marine boundary layer clouds – Part II: Validation using satellite data. *J. Atmos. Sci.*, **53**, 2304–2316.

Cahalan, R. F., and J. B. Snider, 1989: Marine stratocumulus structure during FIRE. *Remote Sens. Environ.*, **28**, 95–107.

Cahalan, R. F., W. Ridgway, W. J. Wiscombe, T. L. Bell and J. B. Snider, 1994: The albedo of fractal stratocumulus clouds. *J. Atmos. Sci.*, **51**, 2434–2455.

Cahalan, R. F., et al., 1999: First international workshop on the intercomparison of three-dimensional radiation codes, Tucson, AZ, November 17–19, 1999.

Chambers, L., B. Wielicki, and K. F. Evans, 1997: Accuracy of the independent pixel approximation for satellite estimates of oceanic boundary layer cloud optical depth. *J. Geophys. Res.*, **102**, 1779–1794.

Cowan, G., 1998: *Statistical data analysis*. Clarendon Press, Oxford, UK. 197 pp.

Davies, R., 1984: Reflected solar radiances from broken cloud scenes and the interpretation of satellite measurements. *J. Geophys. Res.*, **89**, 1259–1266.

Davis, A., A. Marshak, W. Wiscombe, and R. Cahalan, 1994: Multifractal characterizations of non-stationarity and intermittency in geophysical fields: Observed, retrieved, or simulated. *J. Geophys. Res.*, **99**, 8055–8072.

Davis, A., A. Marshak, R. Cahalan, and W. Wiscombe, 1997: The Landsat scale-break in stratocumulus as a three-dimensional radiative transfer effect, implications for cloud remote sensing. *J. Atmos. Sci.*, **54**, 241–260.

Diner, D. J., et. al., 1999: New directions in Earth observing: Scientific applications of multiangle remote sensing. *Bull. Amer. Meteor. Soc.*, **80**, 2209–2228.

Evans, K. F., S. McFarlane, and W. Wiscombe, 2000*: A Stochastic Cloud Field Model for Generalizing Radar Derived Cloud Structure for Solar Radiative Transfer Calculations*. 10th Annual Atmospheric Radiation Measurement program science team meeting, San Antonio, TX, March 13–15, 2000.

King, M. D., W. P. Menzel, P. S. Grant, J. S. Myers, G. T. Arnold, S. E. Platnick, L. E. Gumley, S. C. Tsay, C. C. Moeller, M. Fitzgerald, K. S. Brown and F. G. Osterwisch, 1996: Airborne scanning spectrometer for remote sensing of cloud, aerosol, water vapor and surface properties. *J. Atmos. Oceanic Technol.*, **13**, 777–794.

King, M. D., S.-C. Tsay, S. Platnick, M. Wang, and K.-N. Liou, 1997: *Cloud retrieval algorithms for MODIS: Optical thickness, effective particle radius, and thermodynamic phase.* MODIS Algorithm Theoretical Basis Document No. ATBD-MOD–05, Version 5, NASA.

Knyazikhin, Y., et al., 1998a: Estimation of vegetation canopy leaf area index and fraction of absorbed photosynthetically active radiation from atmosphere-corrected MISR data. *J. Geophys. Res.*, **103**, 32,239–32,256.

Knyazikhin, Y., Y. Zhang, Y. Tian, N. Shabanov, and R. B. Myneni, 1998b: Radiative transfer based synergistic MODIS/MISR algorithm for the estimation of global LAI & FPAR. MODIS semi-annual report: January 01, 1998 – June 30, 1998 (Contract NAS5-96061)

Kobayashi, T., 1993: Effects due to cloud geometry on biases in the albedo derived from radiance measurements. *J. Climate*, **6**, 120–128.

Li, J., D. J. Geldart, and P. Chylek, 1994: Solar radiative transfer in clouds with vertical internal inhomogeneity. *J. Atmos. Sci.*, **51**, 2542–2552.

Loeb, N. G., and R. Davies, 1996: Observational evidence of plane parallel model biases: Apparent dependence of cloud optical depth on solar zenith angle. *J. Geophys. Res.*, **101**, 1621–1634.

Loeb, N. G., and J. A. Coakley, 1998: Inference of marine stratus cloud optical depths from satellite measurements: Does 1D theory apply? *J. Climate*, **11**, 215–233.

Loeb, N. G., T. Várnai, and R. Davies, 1997: Effect of cloud inhomogeneities on the solar zenith angle dependence of nadir reflectance. *J. Geophys. Res.*, **102**, 9387–9395.

Marshak, A., A. Davis, R. F. Cahalan, and W. J. Wiscombe, 1994: Bounded cascade models as non-stationary multifractals. *Phys. Rev. E*, **49**, 55–69.

Marshak, A., A. Davis, W. Wiscombe, and R. Cahalan, 1997: Scale-invariance of liquid water distributions in marine stratocumulus, Part 2 – Multifractal properties and intermittency issues. *J. Atmos. Sci*, **54**, 1423–1444.

Marshak, A., A. Davis, W. J. Wiscombe, and R. F. Cahalan, 1998: Radiative effects of sub-mean free path liquid water variability observed in stratiform clouds. *J. Geophys. Res.*, **103**, 19557–19567.

Nakajima, T. Y. and M. D. King, 1990: Determination of the Optical Thickness and Effective Particle Radius of Clouds from Reflected Solar Radiation Measurements. Part I: Theory. *Journal of the Atmospheric Sciences*, **47**, 1878–1893.

Oreopoulos, L., A. Marshak, R. F. Cahalan, and G. Wen, 2000: Cloud 3D effects evidenced in Landsat spatial power spectra and autocorrelation functions. *J. Geophys. Res.*, in press.

Pincus, R., M. Szczodrak, J. Gu, and P. Austin, 1995: Uncertainty in cloud optical depth estimates made from satellite radiance measurements. *J. Climate*, **8**, 1453–1462.

Platnick S., 1997: The scales of photon transport in cloud remote sensing problems. In *IRS'96: Current Problems in Atmospheric Radiation*, Eds. W. L. Smith and K. Stamnes, Deepak Publ., Hampton (Va), pp. 206–209.

Schertzer, D., and S. Lovejoy, 1987: Physical modeling and analysis of rain and clouds by anisotropic scaling multiplicative processes. *J. Geophys. Res.*, **92**, 9693–9714.

Twomey, S., 1977: *Introduction to the mathematics of inversion in remote sensing and indirect measurements*. Elsevier Publishing Co., Amsterdam, The Netherlands. 243 pp.

Várnai, T., 2000: Influence of three-dimensional radiative effects on the spatial distribution of shortwave cloud reflection. *J. Atmos. Sci.*, **57**, 216–229.

Várnai, T., and R. Davies, 1999: Effects of cloud heterogeneities on shortwave radiation: Comparison of cloud-top variability and internal heterogeneity. *J. Atmos. Sci.*, **56**, 4206–4223.

Vicsek, T., 1989: *Fractal growth phenomena*. World Scientific Publishing Co., Singapore, 97 pp.

Zuidema P. and K. F. Evans, 1998. On the validity of the Independent Pixel Approximation for the boundary layer clouds observed during ASTEX. *J. Geophys. Res.*, **103**, 6059–6074.

Tables

Table 1. Ranges considered for various parameters of cloud optical thickness variability.

Parameter *H*	0.25 - 0.5
Probability of partial cloud coverage	0.5
Cloud fraction for broken cloud scenes	≥ 0.7
Scene-averaged optical thickness	5.0 - 20.0
$\nu=(\text{Mean/Stdev})^2$ overcast scenes broken cloud scenes	2.0 - 25.0 0.5 - 4.0
Shape of optical thickness histogram	Modified Gamma distributions

Figure captions

Figure 1. Root-mean-square (RMS) error of optical depth retrievals. The dashed line shows the errors when all the relevant physical processes are fully represented in retrievals based on 1D radiative transfer theory (1D real clouds). Note that the RMS tends to zero as the observational accuracy increases, indicating that this situation is a "well-posed" problem. In contrast, the solid line corresponds to 3D real clouds, and the RMS does not tend to zero even for perfectly accurate observations. This is an "ill-posed" problem (Twomey 1977). The figure is based on a sample set of radiative transfer calculations carried out at 250 m resolution for 60° solar zenith angle.

Figure 2. Example for estimating the uncertainty of τ-retrievals at 1 km resolution. The error bars indicate the estimated standard deviation of retrieval errors, which, assuming a Gaussian frequency-distribution of retrieval errors, contain the true τ value with a 68% probability. (In Gaussian distributions, the confidence level corresponding to one standard deviation is around 68%.) The solar zenith angle is 60°, and the sun is on the left side.

Figure 3. Comparison of 1D and 3D nadir reflectivities over $(250\ m)^2$ pixels for 60° solar zenith angle. The interval between the two dashed lines schematically illustrates the accuracy of observations.

Figure 4. Dependence of the standard deviation of retrieval errors (σ) of cloud optical thickness on cloud reflectivity. The bold curve shows a polynomial fit of the actual results.

Figure 5. Resolution dependence of retrieval errors. The mean error (μ) is defined simply as $\mu = \frac{1}{N}\sum_{i=1}^{N}\varepsilon_i$, where the individual pixel retrieval error ε_i can be either positive or negative, and σ is defined by Equation (2).

Figure 6. Mean and standard deviation of retrieval errors for various solar zenith angles at 250 m resolution.

Figure 7. Cumulative histogram of retrieval errors defined by Equation (3), for 250 m resolution for 15° and 75° solar zenith angles.

Figure 8. Mean of true optical thicknesses in heterogeneous scenes (3D), and the value retrieved using one-dimensional theory (1D).

Figure 9. Comparison of the $I_{mean}(\tau)$ and the $\tau_{mean}(I)$ curves obtained from averaging over all available pixels in 3D simulations for 60° solar zenith angle and 250 m resolution.

Figure 10. Histogram of true optical thickness values for various reflectivity intervals.

Figure 11. Histogram of the difference between true and retrieved τ values for $I = 0.6$ (continuous curve), and the actual histogram's approximation by a Gaussian distribution that has the same mean and standard deviation (dashed curve). The dotted vertical lines mark the histograms' standard deviation, which is the error bound for 68% confidence level for the Gaussian histogram. The 68% error bounds for the actual histogram are marked by continuous vertical lines.

Figure 12. Absolute values of error bounds for various confidence levels: (a) 95% ("= 1.96 σ"), and (b) 68% ("= 1 σ").

Figure 13. Error estimates for a $(35\ km)^2$ field of marine stratocumulus clouds: (a) original reflectivity field measured at 50 m resolution, and (b) estimated error bounds for optical thickness retrievals carried out at 1 km resolution. The error bonds were set to contain the actual retrieval errors with a 68% probability.

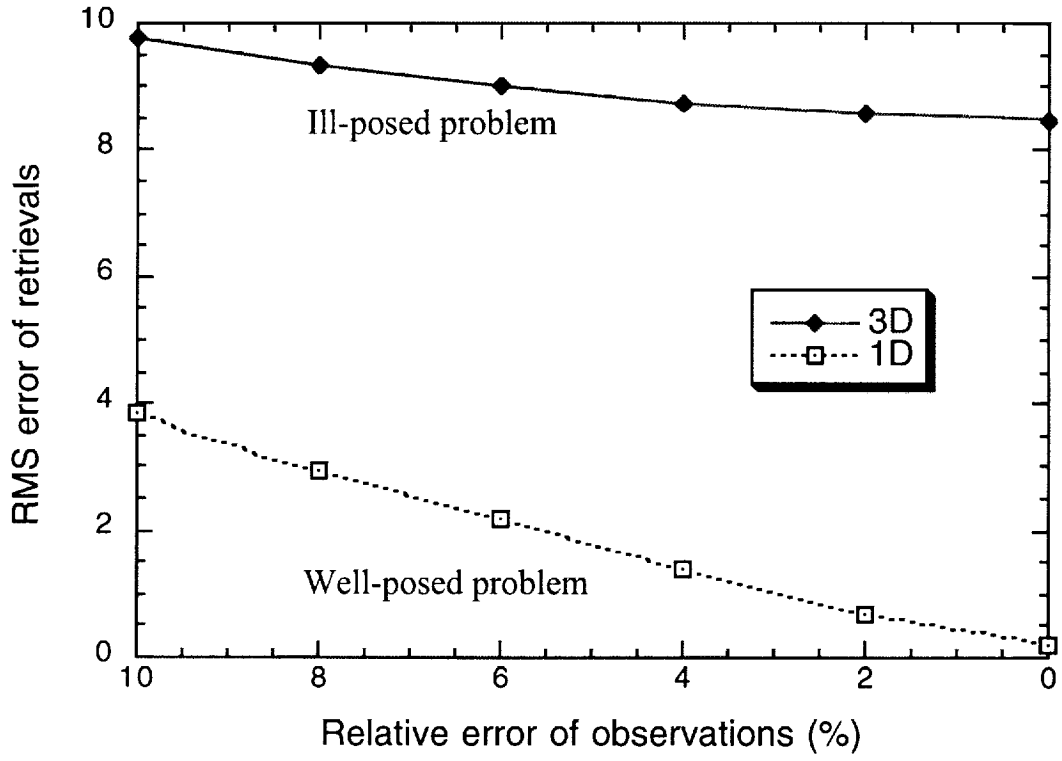
10
8
6
4
2
0
RMS error of retrievals
Ill-posed problem
Well-posed problem
3D
1D
10
8
6
4
2
0
Relative error of observations (%)

Figure 1.

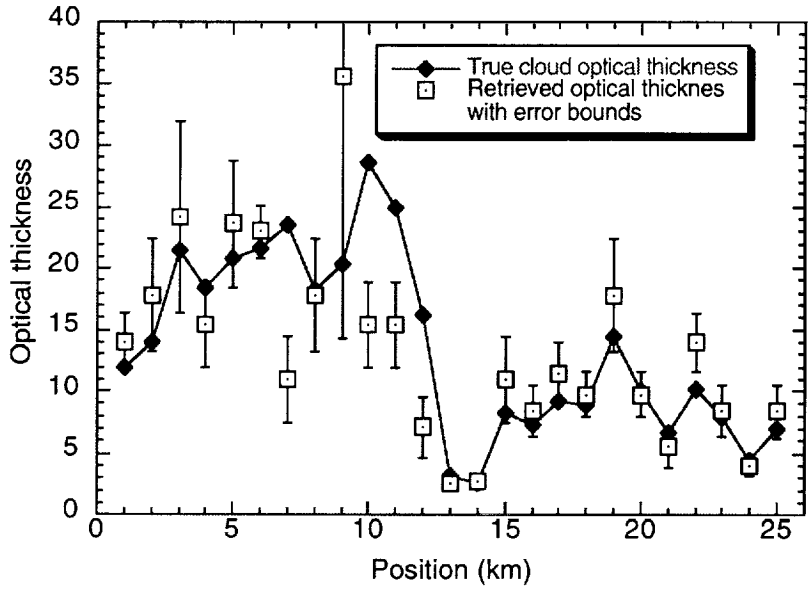
True cloud optical thickness
Retrieved optical thicknes
with error bounds
Optical thickness
Position (km)
0
5
10
15
20
25
30
35
40

Figure 2.

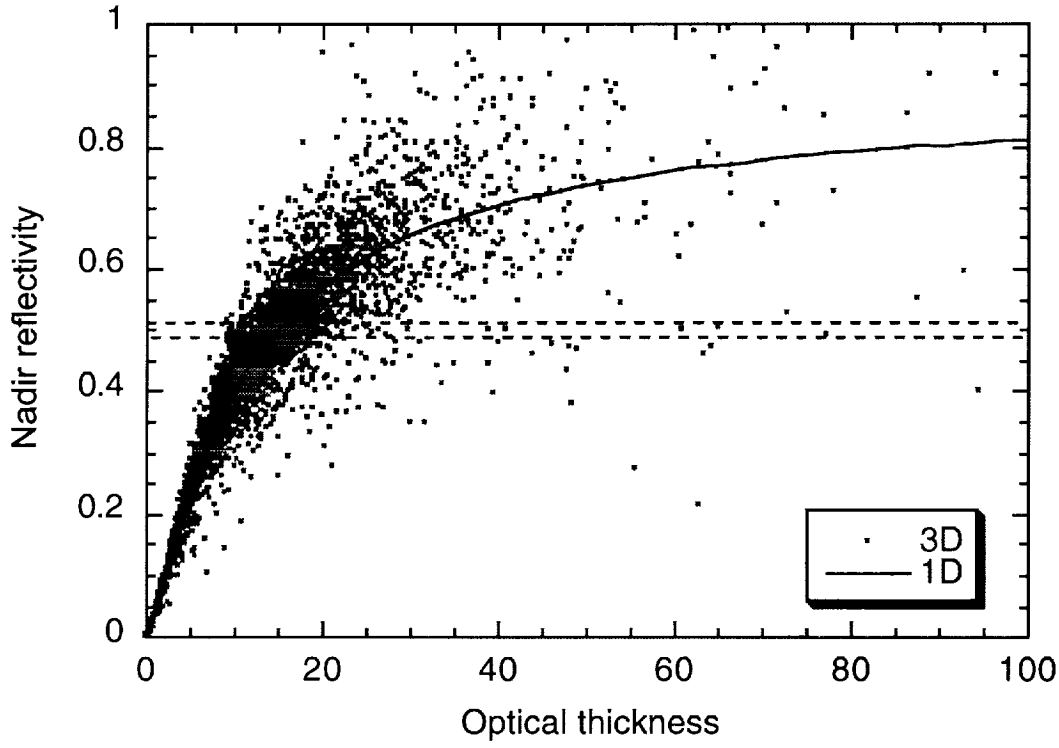
Nadir reflectivity
Optical thickness
0
0.2
0.4
0.6
0.8
1
0
20
40
60
80
100
3D
1D

Figure 3.

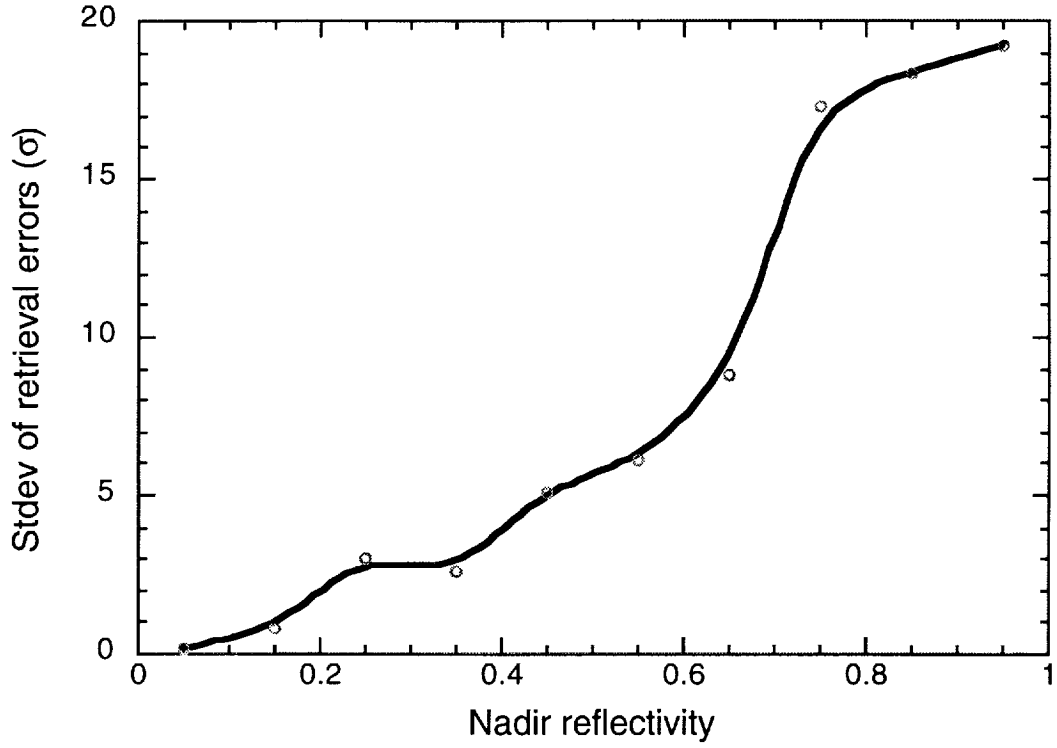
20
15
10
5
0
Stdev of retrieval errors (σ)
0
0.2
0.4
0.6
0.8
1
Nadir reflectivity

Figure 4.

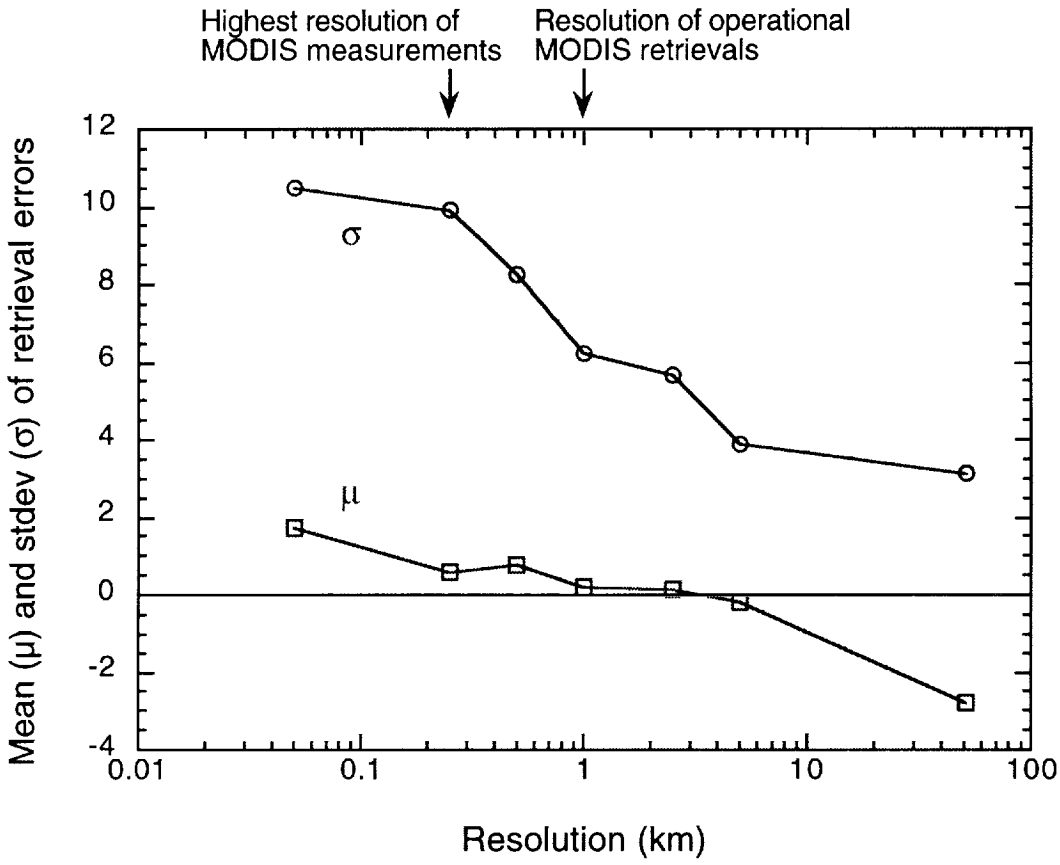
Highest resolution of
MODIS measurements
Resolution of operational
MODIS retrievals
Mean (μ) and stdev (σ) of retrieval errors
12
10
8
6
4
2
0
-2
-4
σ
μ
0.01
0.1
1
10
100
Resolution (km)

Figure 5.

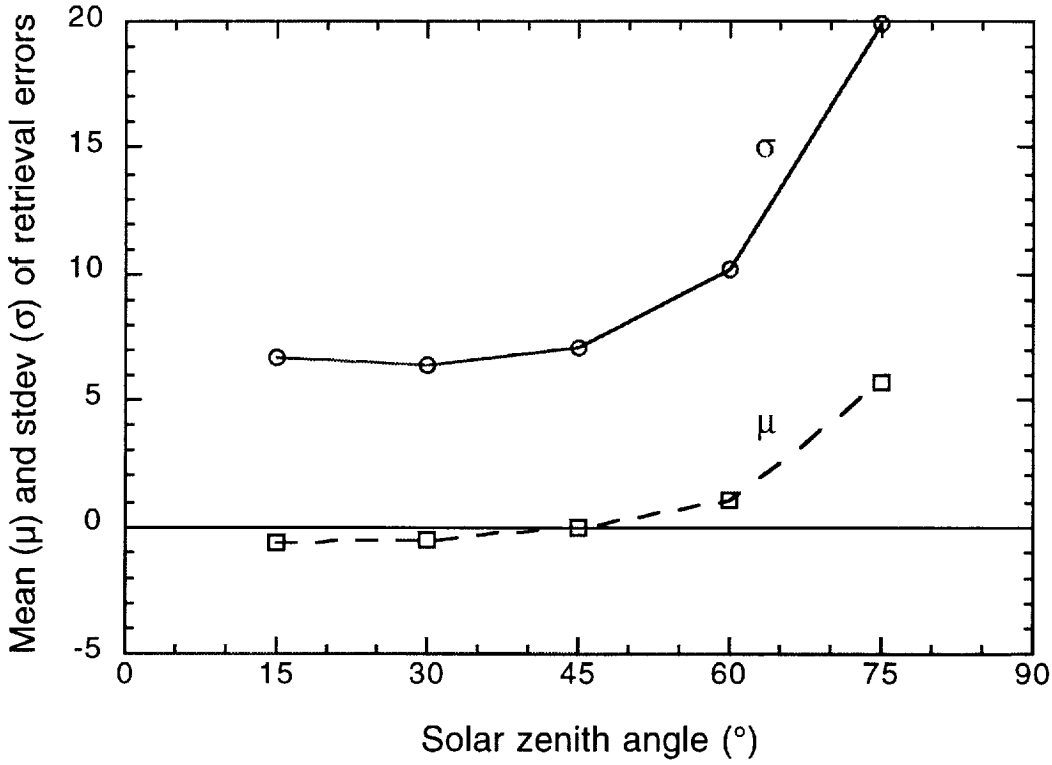
Mean (μ) and stdev (σ) of retrieval errors
20
15
10
5
0
-5
0
15
30
45
60
75
90
Solar zenith angle (°)
σ
μ

Figure 6.

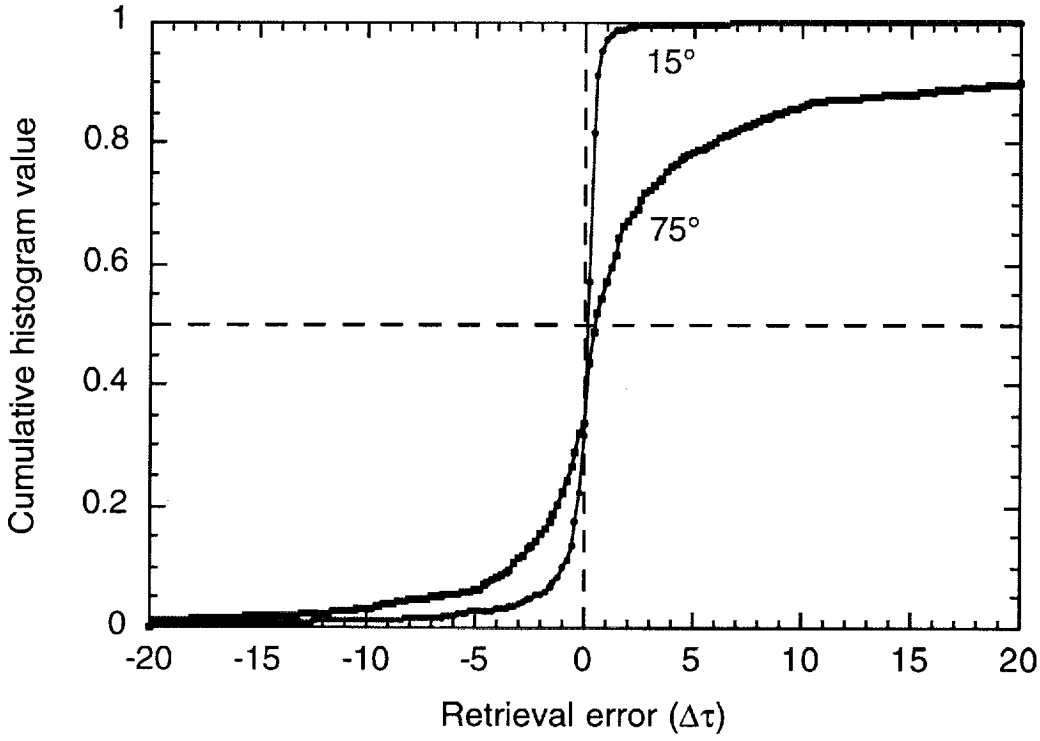
Cumulative histogram value
1
0.8
0.6
0.4
0.2
0
-20
-15
-10
-5
0
5
10
15
20
Retrieval error (Δτ)
15°
75°

Figure 7.

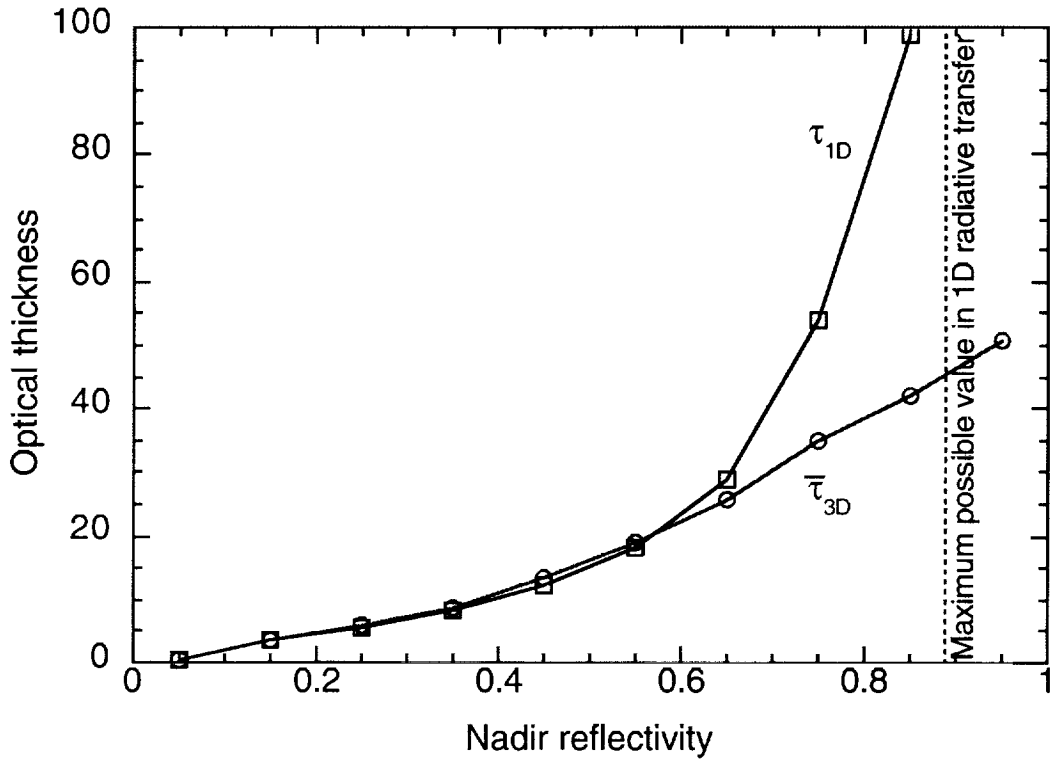
100
80
60
40
20
0
Optical thickness
0
0.2
0.4
0.6
0.8
1
Nadir reflectivity
τ_{1D}
$\overline{\tau}_{3D}$
Maximum possible value in 1D radiative transfer

Figure 8.

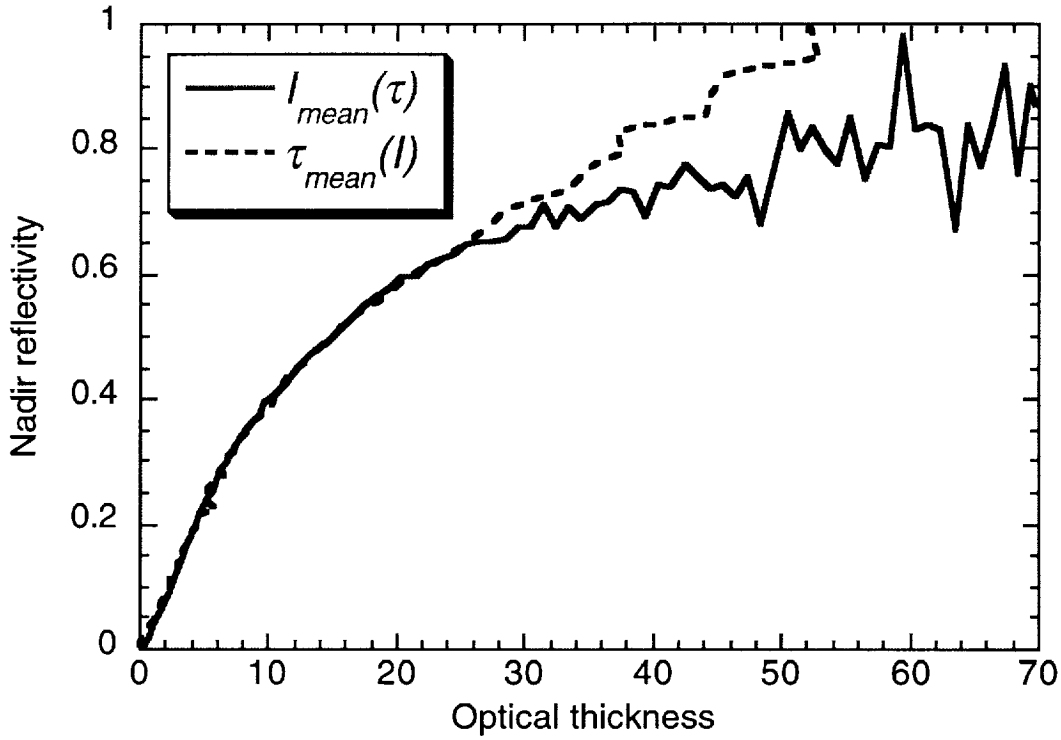
$I_{mean}(\tau)$
$\tau_{mean}(I)$
Nadir reflectivity
Optical thickness
0
0.2
0.4
0.6
0.8
1
0
10
20
30
40
50
60
70

Figure 9.

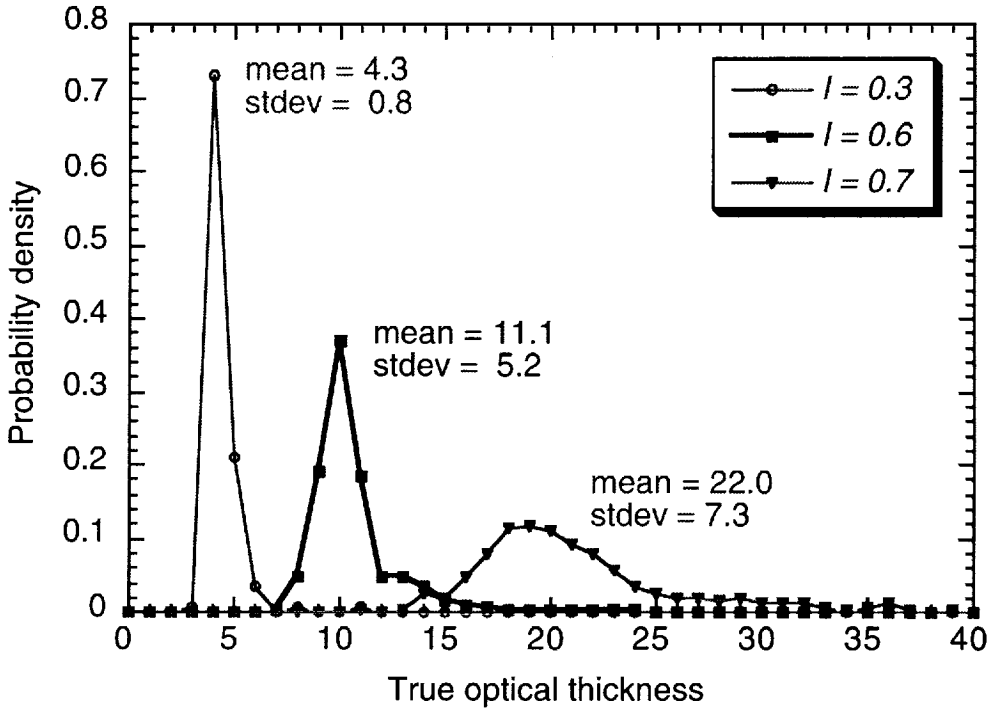
0.8
0.7
0.6
0.5
0.4
0.3
0.2
0.1
0
Probability density
mean = 4.3
stdev = 0.8
mean = 11.1
stdev = 5.2
mean = 22.0
stdev = 7.3
I = 0.3
I = 0.6
I = 0.7
0
5
10
15
20
25
30
35
40
True optical thickness

Figure 10.

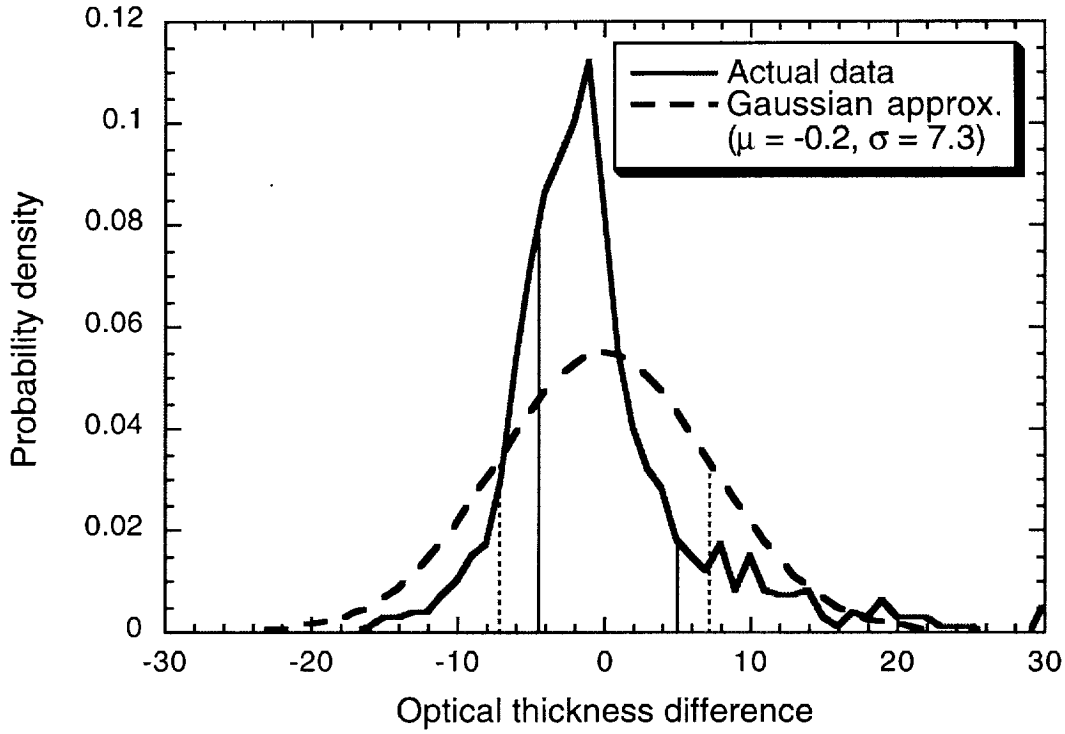
0.12
0.1
0.08
0.06
0.04
0.02
0
Probability density
-30
-20
-10
0
10
20
30
Optical thickness difference
Actual data
Gaussian approx.
(μ = -0.2, σ = 7.3)

Figure 11.

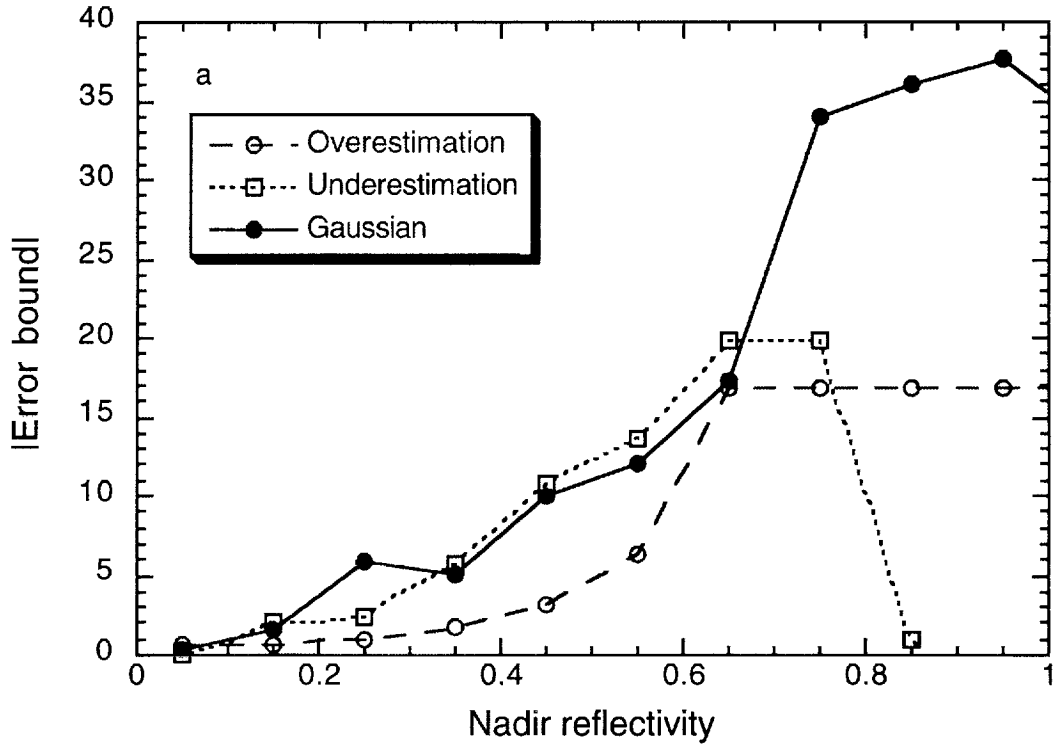
a
Overestimation
Underestimation
Gaussian
|Error bound|
Nadir reflectivity
0
5
10
15
20
25
30
35
40
0
0.2
0.4
0.6
0.8
1

Figure 12a.

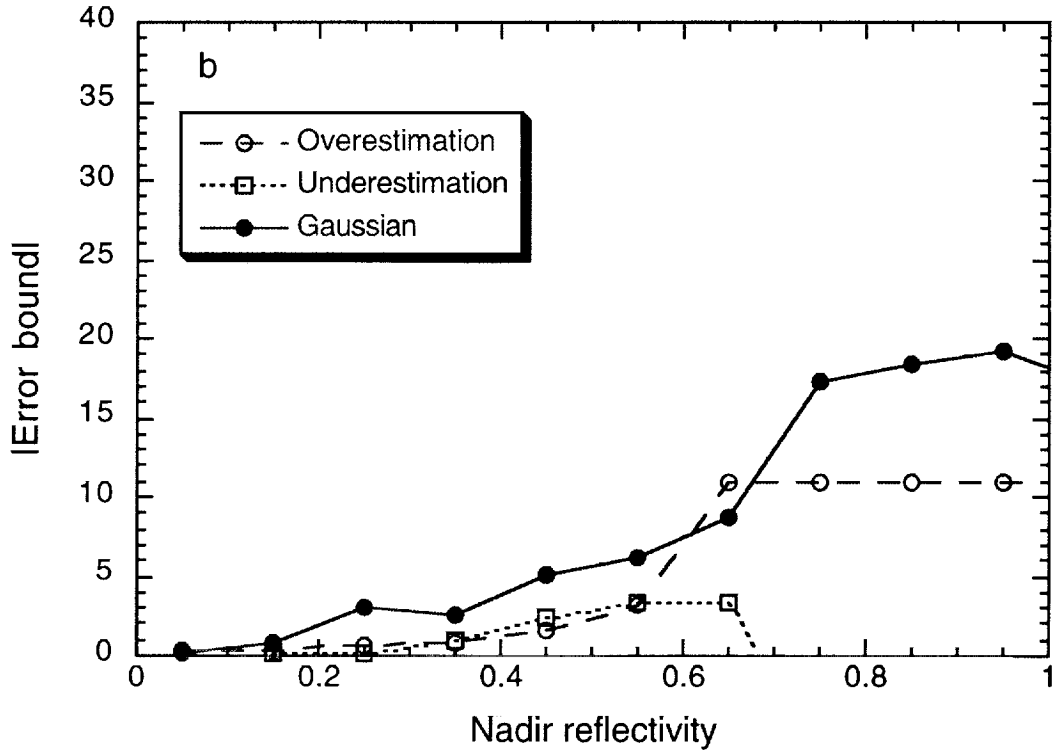
b
Overestimation
Underestimation
Gaussian
|Error bound|
Nadir reflectivity
0
5
10
15
20
25
30
35
40
0
0.2
0.4
0.6
0.8
1

Figure 12b.

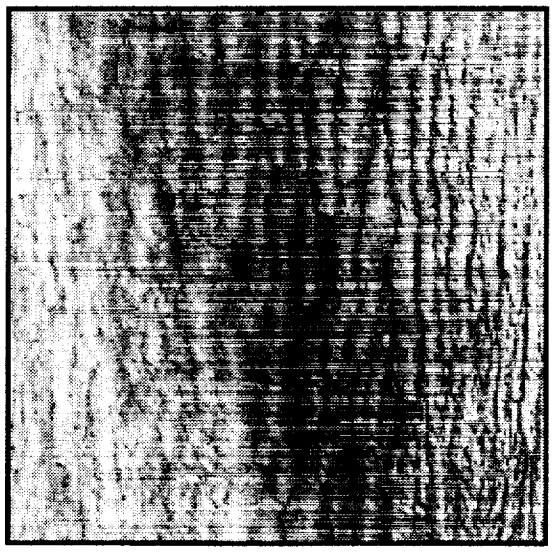

Figure 13a.

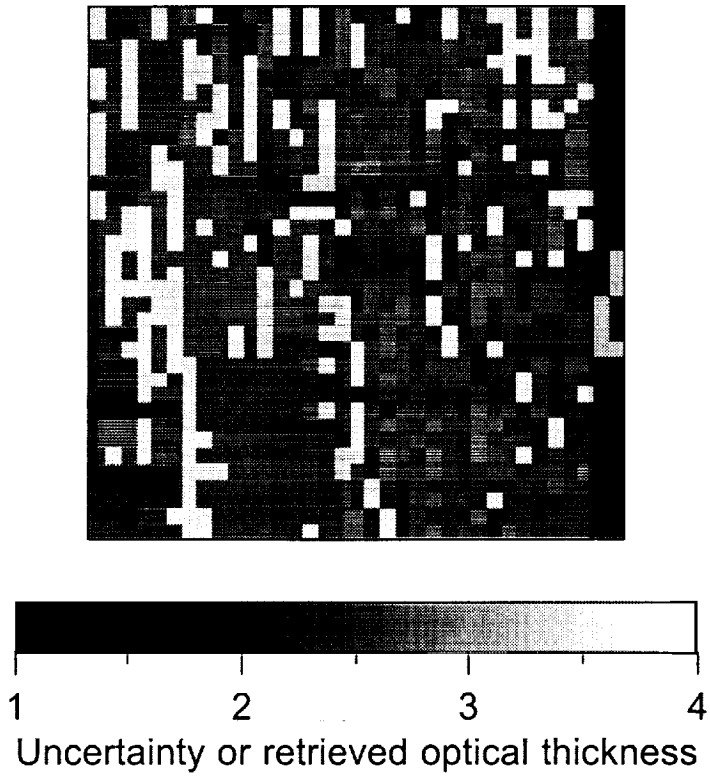

Figure 13b.

Popular summary

Statistical Analysis of the Uncertainties in Cloud Optical Depth Retrievals Caused by Three-Dimensional Radiative Effects

Tamás Várnai and Alexander Marshak

In order to better understand the Earth's atmosphere and to make our predictions about weather and climate more reliable, it is very important to know exactly what clouds are like. Satellites measuring the solar radiation reflected by clouds offer excellent opportunities to determine various cloud properties such as cloud optical thickness. (The optical thickness reveals how easy it is for sunlight to pass through a cloud without being scattered or absorbed by cloud droplets.) This paper presents a simple approach that uses theoretical simulations to estimate the uncertainties that arise in optical thickness retrievals, because current data processing algorithms do not consider how horizontal changes in cloud properties influence the radiation measured at a given point. For the first time, preliminary error bounds are set to estimate the resulting errors for stratocumulus clouds. These estimates can help us better understand the uncertainties that horizontal cloud variability introduces into retrievals of cloud optical thickness, an important product of the Moderate Resolution Imaging Spectroradiometer (MODIS) instrument on board the Terra satellite. The paper also examines how retrieval errors tend to change with known and observable parameters, such as solar elevation or cloud brightness.